- Technical Paper -

NUMERICAL SIMULATION FOR STRESS DISTRIBUTION IN RC BEAMS WITH TOP VFC OVERLAY CONSIDERING INTERFACE CONDITIONS

Elham MAHMOUD [*1] and Tomohiro MIKI [*2]

ABSTRACT

This paper presents an experiment and 3D finite element analysis for stress around cracks at the interface between two materials. The finite element method is used to simulate the stress distribution between NC substrate and VFC overlay, and to provide a comprehensive overview of how stress affects delamination between the two materials under bending loads. Bending test was conducted on wide RC beams repaired with top VFC overlay. FEM results indicate variations in stress at the interface. Additionally, the interface surface condition affected the stress distribution at the point of delamination.

Keywords: VFC overlay, Normal concrete, Interface shear and normal stresses, Stress distribution

1. INTRODUCTION

Infrastructure deterioration due to aging, environmental conditions, or increasing traffic demands requires rehabilitation. Very high strength fiber reinforced cementitious composites (VFC) are new construction materials with high mechanical properties [1]. Note that materials in the high strength range among VFC are known overseas as UHPFRC (ultra-high performance fiber reinforced concrete) and UHPC (ultra-high-performance concrete). It is a promising material for retrofitting that enables extending the service life of bridges, but it still lacks design requirements. VFC is a cementitious material mixed with steel fibers. The components of UHPC typically include Portland cement, silica fume, fine sand, water, a superplasticizer, and steel fibers [2]. Water/cement ratio ranges from 0.14 to 0.22 [3]. UHPC has exceptional mechanical properties with a compressive and splitting tensile strength greater than 150 and 5 MPa, respectively [4]. Steel fibers are added to the VFC mixture in a 1-3% range by volume [5]. Among these materials, VFC covers a wide range of fiber-reinforced cementitious materials, of which the minimum compressive strength is set at 60 MPa [1].

A bridge deck overlay in the United States occurred in May 2016 on a reinforced concrete slab bridge in Brandon, Iowa. A field study was carried out to investigate the interface bond [6]. The bond between the substrate and overlay is an important parameter in understanding the repaired lifespan of the structure. So far, studies have been focused on slant shear tests or perfect bond interface estimation at the beam. Little is known, however, about the FE study with reliable parameters for the interface for the RC beam with VFC overlay. Moreover, it did not show the hidden cracks and stress through the beam section to explain why separation may occur. Therefore, the present study provides a comprehensive overview of how stress distribution at the interface affects delamination between the two materials under bending loads. This study set realistic and reasonable interface parameters, such as cohesion and friction angle values. The effect of substrate surface conditions on delamination is also investigated. The analysis focuses on initial cracking, debonding failure, and/or yielding point. The results of this study will be innovative later for bridge decks using VFC overlay to determine an optimized overlay thickness without overestimating interface criteria.

2. EXPERIMENTAL PROGRAM

A four-point bending test was conducted on beams top-repaired by VFC. The specimen cross-sections and reinforcement detailing specifications are illustrated in Fig.1. The beam cross-section measured 200 mm in total depth, 400 mm in width, and 150 mm in effective depth, with a shear span of 550 mm. The thickness of the top-repaired VFC layer was 20 mm and 50 mm, referred to as WU-20 and WU-50, respectively. Three D13 steel reinforcement bars, with a yield strength of 370 MPa, were placed on the tension side, while two D6 bars were used on the compression side. The distance between the two concentrated loads was 150 mm. These beams were tested to simulate the behavior of a repaired bridge deck under flexural loads.

Table 1 summarizes the experimental datasets. Compressive strength was 40.5 MPa for normal concrete and 117.3 MPa for VFC, respectively. The tensile strength was 2.9 MPa for NC and 11.1 MPa for VFC using a cylindrical tensile splitting test. Young`s modulus was 33.5 GPa for normal concrete and 45.9 GPa VFC, respectively.

During the testing phase, the structural behavior of the beams was measured by recording the loads, vertical displacements, and strain changes at the reinforcement, interface, and VFC layer. The applied load was controlled and gradually increased until failure occurred.

*1 Ph.D student, Dept. of Civil Engineering, Kobe University, JCI Student Member
*2 Associate Prof., Dept. of Civil Engineering, Kobe University, Dr.Eng., JCI Member

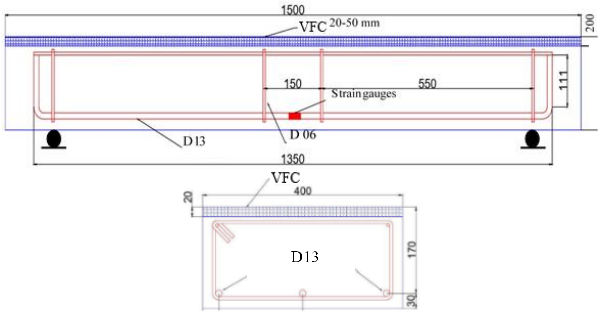

Fig.1 Beam Dimensions (in mm)

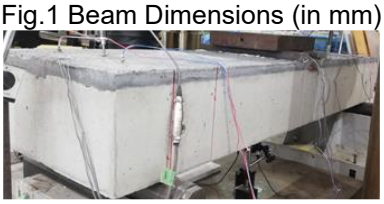

Fig.2 Test setup

Table 1 Mechanical properties of NC and VFC

	f'_c	f_t	E_c
	MPa		GPa
NC	40.5	2.9	33.5
VFC	117.3	11.1	45.9

Vertical displacement was measured using two transducers placed along the middle span for maximum measurement and at both supports to evaluate displacements in the opposite direction. One strain gauge was installed at the top mid-span of the VFC layer, while two were positioned on the side of the beam at the repaired layer. Deflections and mechanical strains were recorded at each load step. Six plastic strain gauges with 50 mm length were embedded at the interface surface between NC-VFC. Two were positioned at the left and right supports, and two were in the middle of each beam, as shown in Fig.2.

3. MODELING

3.1 Materials

Nonlinear FEM software Diana version 10.10 was used. 3D FE modeling was conducted to understand the influence of using VFC overlay on the concrete stress distribution and the arrest of cracking. 3D solid quadrilateral elements with eight nodes were used for NC, VFC, and steel plates with a meshing size of 20 mm, as depicted in Fig. 3. The model coordinate system was used where the X-axis was for longitudinal length (1500 mm), the Y-axis was for width (400 mm), and the Z-axis was for depth (200mm), respectively.

3D solid quadrilateral elements with a nodes model were used for concrete as expected different stress distributions along the beam's width. NC and VFC were modeled using the total strain-based crack model. The tensile behavior was described with a smeared crack model. Both the NC and VFC models utilized a parabolic model for compressive strength (fc) and an exponential model for tensile strength (f_t), as illustrated in Figs.4(a) and 4(b), respectively. The parabolic and exponential model was provided. The experimental material properties, such as compressive stress and tensile stress to NC and VFC, were used as a FEM data set, as shown in Tables 1 and 2. Tensile feature energy (G_F) to VFC

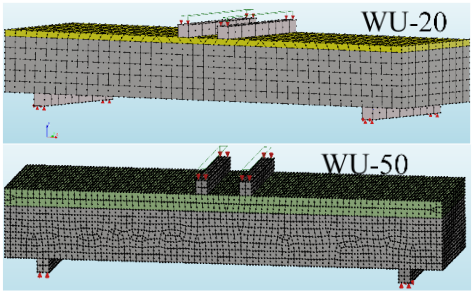

Fig.3 FE discretization with boundary condition.

Table 2 Beam FEM parameters

NC	E_c 33000 MPa, ν 0.15, f'_c 40 MPa, f_t 2.9 MPa, G_F 0.09 N/mm.			
VFC	E_{VFC} 45000 MPa, ν 0.15, f'_c 117 MPa, f_t 11 MPa, G_F 20 N/mm.			
Reinforcing bar(tension)	E_s 200000 MPa, f_y 370 MPa, f_{ult}. 530 MPa			
	K_n 33000 N/ mm^3			
			G	**P**
Interface (NC-VFC)	**Nonlinear elastic friction**	K_s	10	0.01
		C (MPa)	1.5	0
		ϕ (°)	60	60

was set as an assumption based on another numerical model based on our experimental results using steel fiber concrete overlay. G_F affects the load-displacement curve but does not affect interface behavior. For WU 20 and 50 FE models, G_F was assumed to range between 3 and 20 N/mm. As for WU-20, G_F of 3 N/mm was acceptable, while WU-50 was not enough, as discussed in results in 4.2. Therefore, in this study, the value G_F was taken as 20N/mm for WU-20 and WU-50. The nonlinear material properties of the steel reinforcement were defined according to the Von Mises criteria, as shown in Fig. 4(c). The steel plates were modeled using an elastic isotropic law, with an elastic modulus (E_s) of 200 GPa and a Poisson's ratio (ν) of 0.3. Steel plates were used as supports and loading plates. The boundary conditions for the supports were a roller and hinged. The linear interface was used to connect supports and NC, and also the loading plates and VFC layer. The load was applied as a displacement control step, and the regular Newton-Raphson iterative method was used to calculate the structural response. The Maximum number of iterations was set as 10.

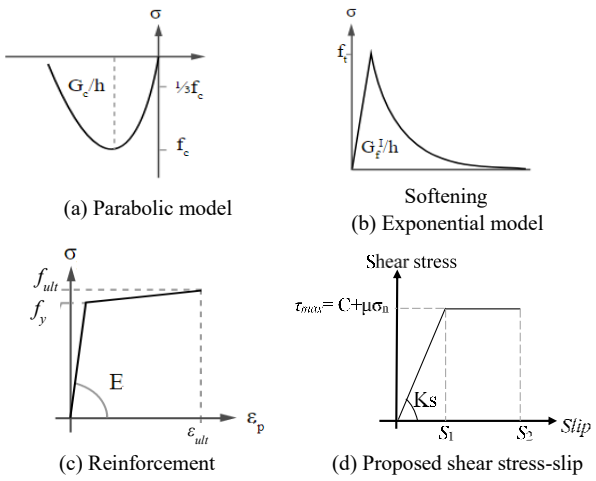

Fig.4 Constitutive models

3.2 Interface element

The parameters of the interface models were determined to reach an agreement between the load-deflection curves and experimental behavior. Two FE model sets were obtained considering the interface conditions: poor and good adhesion conditions for the good adhesion condition (noted as G). It reflects that failure at the interface occurred at the ultimate peak load in limited spots at the interface surface. In contrast, a dry substrate interface was simulated as a poor adhesion condition (noted as P). It reflects that interface failure occurred at early loading stages pre-peak load and with a wide range of interface surfaces.

A nonlinear elastic friction interface material type was employed, focusing primarily on the normal and shear stresses at the interface. The interface element's normal stiffness modulus, Kn (N/mm³), and shear stiffness modulus, Ks (N/mm³), were used with initial values for different interface types. The normal stiffness modulus corresponds to the NC compressive Youngs modulus. In contrast, the shear stiffness has a wide range that aligns with laboratory results, setting the initial slope of the shear stress-slip relationship, as illustrated in Fig. 4(d). This slope varies based on the interface conditions and good or poor substrate surface conditions. In the proposed shear stress-slip relationship, S_1 is the slip at the end of elastic behavior, and S_2 is the shear ultimate slip.

For simplicity of the illustration, the 2D model is used for the explanation. Every node at the corners of the material element square has strains and displacements in both the x and y directions. The nodes along the middle line interface only have displacements in the x and y directions. The 2D quadratic line interface element consists of six nodes (1, 5, 2) and (13, 16, 12), representing two surfaces with zero thickness. The interface nodes interact with the bulk of the adjacent elements, as illustrated in Fig. 5. In the experimental study, the delamination occurred with later movement to overlay from one side of the beam at the peak load. NC-VFC interface in the tested beams was used without anchors and epoxy resin. This interface was assumed to be evaluated by Eq. (1) in this study.

$$\tau = C + \mu\,\sigma_n = \mathrm{C} + \sigma_n \tan\phi \qquad (1)$$

where, τ is the peak shear stress, C is the cohesion stress, μ is the coefficient of friction, σ_n is the stress normal to the shear plane, and ϕ is the friction angle.

AASHTO provides the values of C and μ on the NC-NC interface with different roughness of the substrate surface, i.e., 1.65 MPa and 1.0 for the rough surface. This study set these values based on try-and-error trials. The FE parameters for good and poor surface conditions are summarized in Table 2. The NC-VFC interface used a nonlinear elastic friction model, simplifying the Coulomb friction model.

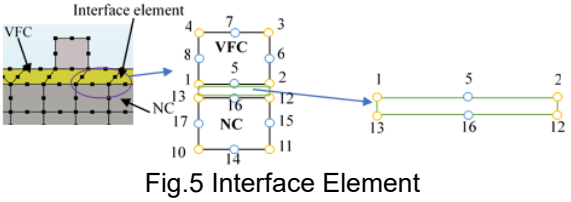

Fig.5 Interface Element

The ACI Committee 224 specifies permissible crack widths for reinforced concrete under service loads, with limits ranging from 0.1 mm to 0.41 mm, depending on exposure conditions. In our study of target bridge decks, cracks tend to grow due to the influence of traffic loading. For simplicity, it is assumed that an interface vertical opening value of 0.1 mm, equivalent to 2000 μ strain in the 50 mm length gage, defines an interface delamination in the analytical results. However, during the experimental study, delamination was indicated when the strain gauges at the interface were cut due to separation.

4. RESULTS AND DISCUSSION

4.1 Experimental Results

Figure 6 illustrates the flexural load-deflection response of WU-20 and WU-50 across several phases. WU-20 beam, flexural cracks were initiated at an applied

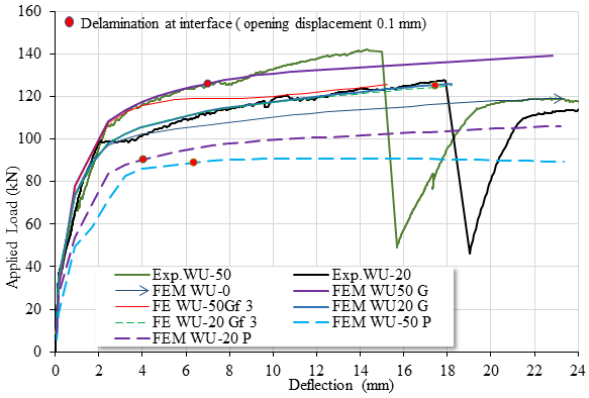

Fig.6 WU-20/50 experiment & FE Load-deflection

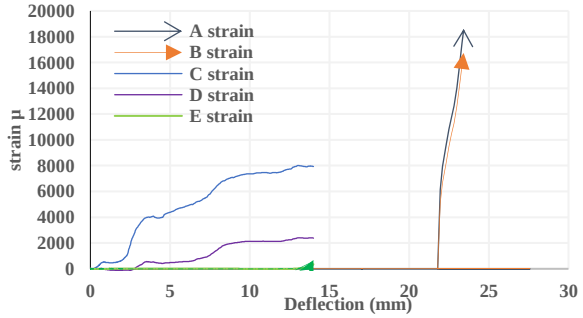

(a) WU-50

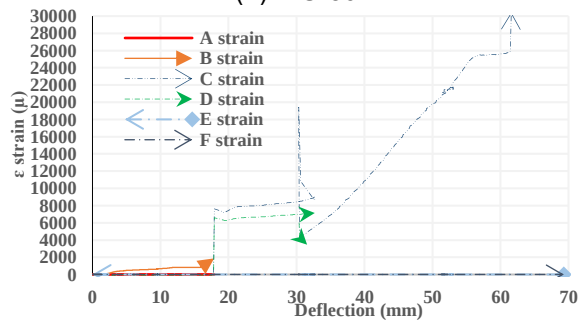

(b) WU-20

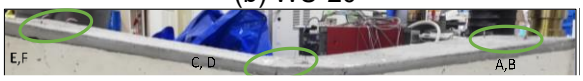

(c) Location of embedded gages

Fig.7 Tensile strain at NC-VFC interface

load of 35 kN. These cracks were vertical and located at the bottom middle span of the beam. As the load increased, flexural cracks propagated at the pure bending zone. Upon reaching the yield point at 95 kN and 3.9 mm displacement, the cracks extended to the NC and VFC overlay interface. From the yielding stage to the peak load at 127 kN with 17.7 mm displacement, horizontal cracks at WU-20 developed until the strain gauges between the NC and VFC could detect delamination. At peak load point, a loud with lateral movement to overlay occurred.

For WU-50, The first phase was the linear elastic, and the second phase corresponds to the cracking stage, where bending cracks were initiated, but the longitudinal reinforcing steel had yet to yield. The initial bending cracks appeared at the bottom midspan when the load reached 30 kN. The next phase involves yielding of the longitudinal reinforcing steel at 112 kN. As the applied load increases, aloud sound is headed at interface separation after the peak load of 142.1 kN at 14.6 mm displacement and the midspan deflection of 15 mm, as shown in Fig.6. This is followed by the failure phase. The cracks in the WU-50 were significantly finer compared to those in the WU-20, up to 80% of the peak load. WU-20/50 failure mode was flexural with the yielding of the reinforcing steel.

The NC-VFC interface delamination became quite pronounced immediately at the peak load. In the delamination for WU-20, four out of six strain gauges were cut at peak load, as shown in Fig. 7(b). The same was for WU-50 but the changes in reading for one of the middle beam gauges started in early loading stage, as shown in Fig.7(a). The location of the strain gauges is shown in Fig.7(c). The results showed an increase in peak load with increasing overlay thickness compared to the FE result for the beam without overlay (WU-0), which was 119 kN.

4.2 FEM Analysis Results

(1) NC-VFC interface with good interface condition

Figure 6 illustrates the load-deflection curves, showing that the experimental results align closely with the FE analysis. The peak loads of beams are acceptable compared to the experimental data presented in Table 3. WU-0 was simulated using FEM to show the effectiveness of the VFC overlay usage. The accuracy values, calculated as the maximum load from the analytical results divided by the maximum experimental load and the FEM analysis results, can predict the experimental study outcomes with 100% and 97% for WU-20, and WU-50, respectively. FE results are shown as slices just 1mm under and above the interface plane. It is used to study the stress distribution for NC and VFC. FE results are represented as the Cauchy total stresses at the global direction in X direction represented as SXX. The positive values refer to tensile stress, and the negative refers to compressive stress. The interface relative displacement results in the Z direction named DUZ. The positive values refer to opening (tension), while the negative values refer to closing (compression). The separation at the interface occurred when the value of interface relative displacement (DUZ) reached 0.1mm.

Table 3 Experimental and FEM peak loads

Specimen ID	Peak load (kN)		
	Pmax_Exp	Pmax_ana	$\frac{P_{max\_ana}}{P_{max\_exp}}$
WU-0	-	119.0	-
WU-20G	128.0	127.9	1.00
WU-50G	142.1	138.9	0.97

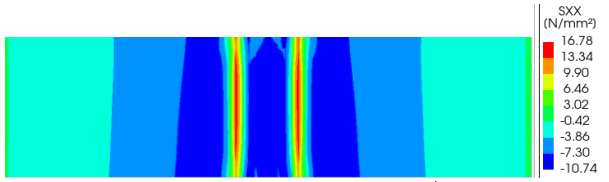

(a) VFC bottom stress distribution at 1st VFC cracking.

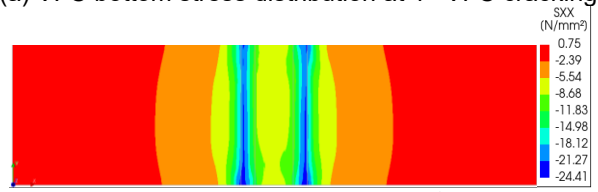

(b) NC upper face stress distribution at1st VFC cracking.

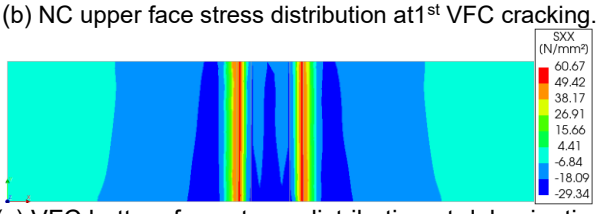

(c) VFC bottom face stress distribution at delamination

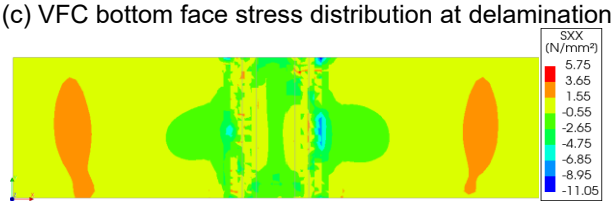

(d) NC upper face stress distribution @ delamination

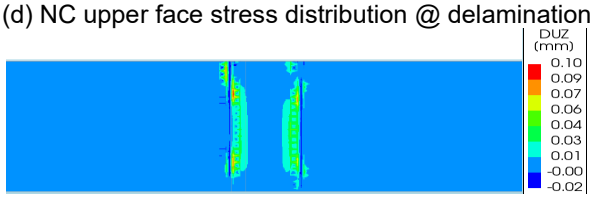

(e) Interface opening distribution at delamination

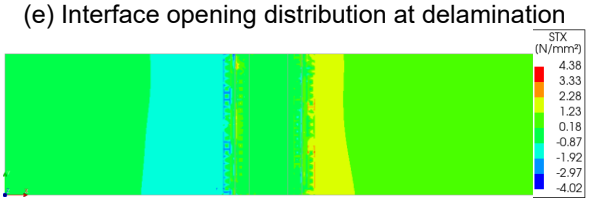

(f) Interface shear stress at delamination

Fig. 8 Analytical results for WU-20G

The interface total tractions in the X direction (interface shear stress) are named STX.

Figure 8(a) illustrates the stress distribution of overlay when cracking is initiated in the VFC. It appeared in the middle of the bottom face of the overlay, specifically under the loading plates on the compression side of the NC. The maximum tensile stress reached 16.78 MPa, while the maximum compressive stress was 10.74 MPa. At the same loading step, the NC maximum tensile stress reached 0.75 MPa, while the maximum compressive stress was 24.41 MPa, as shown in Fig.8(b). At the loading step of the interface vertical opening of 0.1 mm, the VFC maximum tensile stress was 60.67

MPa, while the maximum compressive stress reached 29.34 MPa, as shown in Fig.8(c). NC maximum tensile stress was 5.75 MPa, and compressive stress reached 11.05 MPa.as shown in Fig.8(c). In Fig.8(e), the interface opening distribution indicates that delamination occurred beneath the loading plates with a maximum interface shear stress of 4.38 MPa (Fig.8(f)). Figure 9 illustrates the stress distribution in the WU-50G. When VFC cracked, the maximum tensile stress was 14.39 MPa, mainly shown under loading plates and at pure bending zone, as shown in Fig. 9(a). Meanwhile, the NC at the interface surface remains under compression, with maximum tensile stress at 2.18 MPa and maximum compressive stress at 10.91 MPa, as illustrated in Fig.9(b). At the interface vertical opening of 0.1mm, the tensile stress at the VFC for WU-50G reached 15.56 MPa, while the compression stress was 7.27 MPa, as shown in Fig.9(c). Additionally, Fig.9(d) shows NC stress distribution, mainly in comparison at the same area, while VFC indicates tension. The maximum tensile stress was 8.05 MPa. Figure 9(e) shows the vertical interface opening distribution with a maximum interface shear stress of 3.72 MPa, as shown in Fig. 9(f). Fig. 8(a), (c) show that WU-20G maximum tensile stress distribution was limited under the loading plates while WU-50G had wider distribution across the pure bending zone as shown in Fig.9 (a), (c). At the delamination loading step, it was observed that the interface shear stress was almost very close. The maximum interface shear stress was 4.36 to 3.72 MPa, respectively, which exceeds the interface cohesion stress value of 1.5 MPa. It means that perfect bond cohesion stress could be 4 MPa. And the difference in stresses at the interface between NC and VFC is one of the reasons for the separation.

(2) NC-VFC interface with a poor interface condition

The developed FEM was applied to analyze the poor interface surface condition (P), as detailed in Table 2. At delamination, the maximum tensile stress was 27.64 MPa for WU-20 P, as shown in Fig.10(a). Meanwhile, NC recorded the maximum tensile stress as 0.14 MPa (Fig. 10(b)), with cohesion stress as 0.0067 MPa (Fig. 10(d)). The beam delamination was cross all the pure bending zone as shown in Fig.10(c). For WU50, VFC maximum tension stress was 13.98 MPa. (Fig.11(a)). Meanwhile, NC tensile stress was 0.15 MPa, as shown in Fig.11(b). The interface shear stress was 0.0174 MPa, as shown in Fig.11(d).

A comparison of the results from the good and poor interface FEM revealed important differences in delamination behavior. It was found that delamination occurred at VFC maximum tensile stress of 60.67 MPa for the WU-20G model, as shown in Fig. 8(c). In contrast, delamination for the WU-20P model occurred at a significantly lower VFC tensile stress of 27.20 MPa, as

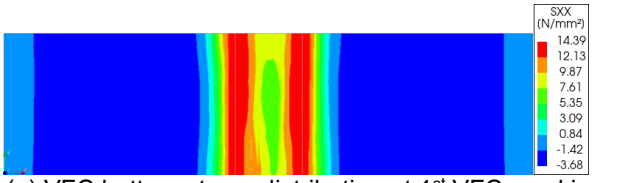

(a) VFC bottom stress distribution at 1st VFC cracking.

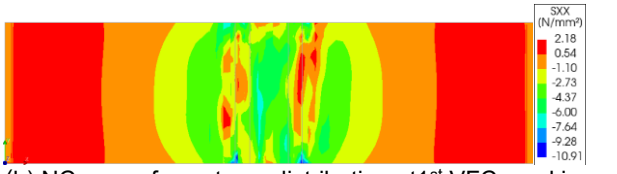

(b) NC upper face stress distribution at1st VFC cracking.

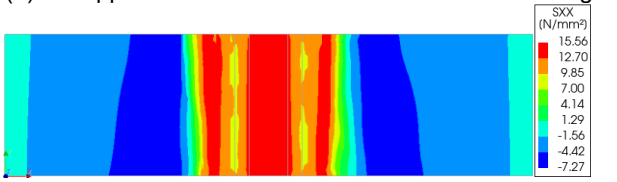

(c) VFC bottom face stress distribution at delamination

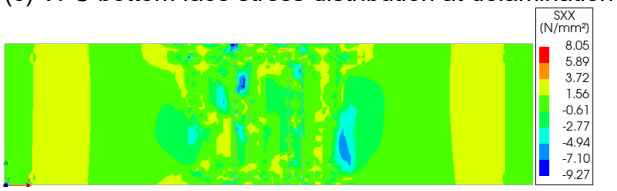

(d) NC upper face stress distribution at delamination

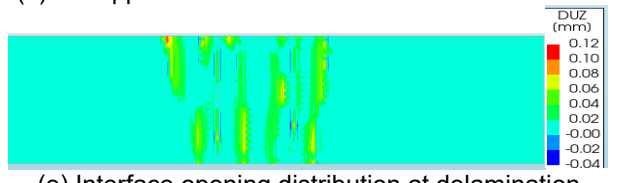

(e) Interface opening distribution at delamination

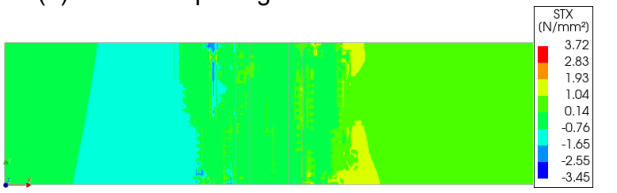

(f) Interface shear stress at delamination

Fig. 9 Analytical results for WU-50G

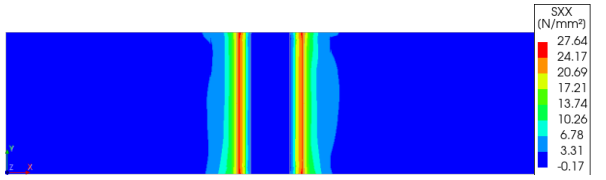

(a) VFC bottom face stress distribution at delamination

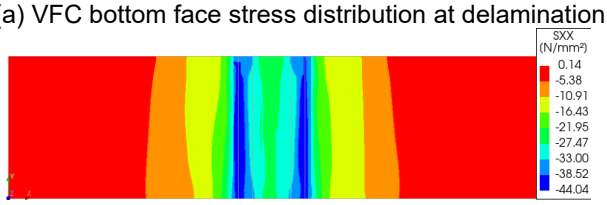

(b) NC upper face stress distribution at delamination

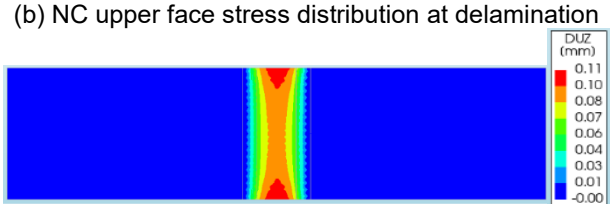

(c) Interface opening distribution at delamination

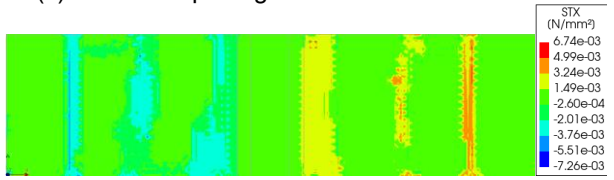

(d) Interface shear stress at delamination

Fig. 10 Analytical results for WU-20P

(a) VFC bottom face stress distribution at delamination

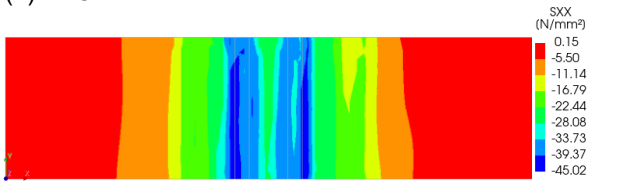

(b) NC upper face stress distribution at delamination

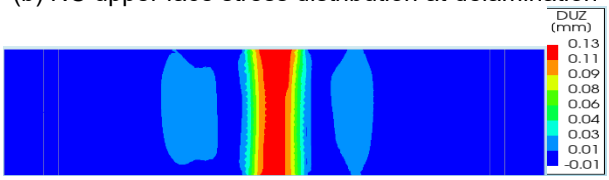

(c) Interface opening distribution at delamination

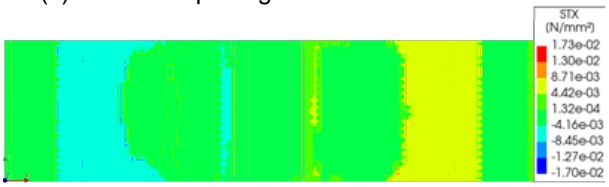

(d) Interface shear stress at delamination

Fig. 11 Analytical results for WU-50P

illustrated in Fig. 10(a). This indicates that poor interface conditions require less energy to initiate delamination. Furthermore, the poor interface model exhibited lower beam stiffness compared to the good interface model, as shown in Fig. 6. The values of cohesion and shear stiffness modulus also play a critical role in influencing results such as the peak load and the onset of early delamination at the interface. The FEM analysis results indicate that the top repaired beam with the VFC overlay, subjected to bending loads, exhibited a varied stress distribution which it can be one of the reasons that delamination occurred. This difference in the stresses creates a scenario where delamination is more likely to occur. A good interface condition leads to delamination at higher debonding stress levels compared with poor case, where delamination occurs at lower stress levels and spreads more broadly across the interface. FE perfect bond cohesion stress could be 4 MPa. Increasing the overlay thickness required less VFC tensile stress for delamination compared to thinner thickness, as shown in Fig.9(a) for WU-50 and Fig.8(a) for WU-20.

5. CONCLUSIONS

The experimental results of the composite beams indicated an improvement in bending strength compared to beams without repair. A suitable interface with good adhesion conditions is used to develop a 3D FE model for the top-repaired reinforced concrete beam with different overlay thicknesses. Another set of parameters was used with poor adhesion to the substrate surface. A nonlinear elastic friction interface type was used, with the normal stiffness set equal to the concrete's Young's modulus. The shear stiffness was established at 10 N/mm³ for good adhesion surface condition and 0.01 N/mm³ for poor condition. The cohesion stress was set at 1.5 MPa for good adhesion surface conditions, while 0 MPa for poor surface conditions. FE results can predict the experimental study outcomes with 100% and 97% accuracy for WU-20 and WU-50, respectively. Due to the high mechanical properties of the VFC, increasing VFC overlay thickness resists bending and works effectively with the NC layer. The interface separation occurred at a wider area compared with thinner overlay thickness. Delamination occurred in poor adhesion surface conditions at early loading stages, with significant low beam stiffness after cracking and yielding. Perfect bond cohesion stress could be 4 MPa. That shows the importance of substrate surface preparation, which should be taken into consideration. The stress distribution at the interface showed compression stress from NC upper side with big VFC tension stress at the same place. The good surface preparation provides better performance compared with the poor case. Therefore, good surface preparation with thinner overlay thickness is recommended in further investigations into full bridge finite element modeling to determine the optimized overlay thickness without overestimation to interface criteria at yielding point or deboning failure.

ACKNOWLEDGEMENT

This research was supported by the Japan Society for the Promotion of Science (JSPS), Grant-in-Aid for Scientific Research (B) JP23K26187, and SIP Smart Infrastructure Management System, Topic e-2: EBPM-based Group Management Technologies.

REFERENCES

[1] JSCE, “Recommendations for Design and Construction of Very High Strength Fiber Reinforced Cementitious Composite Structures (Draft).” Concrete Library 166, Japan Society of Civil Engineers, 2024.

[2] Arora A, Yaob Y, Mobashera B, Neithalath N. “Fundamental Insights into the Compressive and Flexural Response of Binder and Aggregate-optimized (UHPC)”. Cement Concrete Composite, 98, 1-13, 2019.

[3] Shi, C., Wu, Z., Xiao, J., Wang, D., Huang, Z., Fang, Z. “A Review on UHPC Part 1. Raw Materials and Mixture Design.” Construction and Building Materials, 101, 741-751, 2015.

[4] Tayeh, B.A. Abu Bakar, B.H. Johari M.A., Zeyad, A.M., “Microstructural Analysis of the Adhesion Mechanism Between Old Concrete Substrate and UHPFC”, J. Adhes. Sci. Tech. 28 1846-1864, 2014

[5] Wille, K., Kim, D.J., Naaman, A.E. “Strain hardening UHP-FRC with Low Fibre Contents.” Mater Struct, 44(3):583e98, 2011.

[6] Haber, Z.B., Munoz, J.F., Graybeal, B.A. “Field Testing of UHPC Overlay.” Federal Highway Administration, FHWA-HRT-17-096, 2017.